# LAB UNIT 4: Lateral Force Microscopy

## Specific Assignment: Viscoelastic Response and Friction Study

Objective   This lab unit introduces lateral force microscopy in two embodiments, a scanning force microscopy (SFM) based mechanical (sinusoidal) perturbation method referred to as force modulation microscopy, and friction force microscopy (FFM) to explore thermomechanical properties in polymers around the glass transition and friction forces.

Outcome   Learn about the basic principles of contact mechanics and polymer viscoelasticity, friction and conduct force modulation studies as a function of temperature below and above the polymer glass transition.

Synopsis   Lateral force microscopy provides surface sensitive local information about nano-mechanical properties, such as friction coefficient, material stiffness (moduli), hardness, elastic-plastic yield points, and viscosity. As SFM based methods operate with nanoscale probing areas, perturbation-induced material activation into metastable configurations can largely be avoided, which makes force modulation microscopy very sensitive to "true" (equilibrated) material properties. This is illustrated with this project utilizing with small amplitude normal modulations at a variety of temperatures around the glass transition of poly-t-butylacrylate thin films.
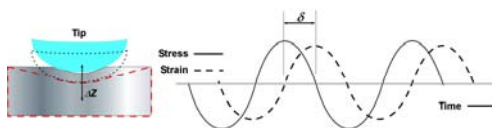
Force modulation spectroscopy applied to local glass transition at polymer surface *(above)* and dependence of friction coefficient on temperature for polystyrene *(right).*
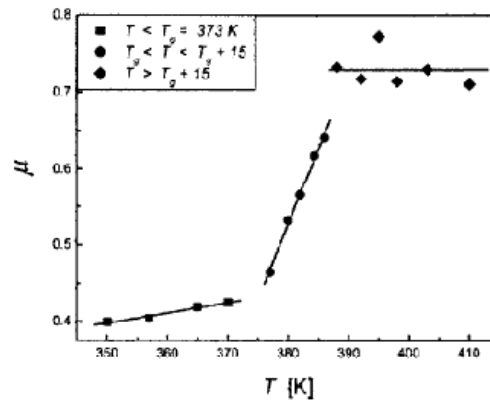
Materials   Poly-t-butylacrylate spin-coated film (> 100 nm) on silicon substrates.

Technique   SFM force modulation microscopy and friction force microscopy

Table of Contents

1. Assignment

The assignment is to locally investigate the nano-thermomechanical properties of thin film polymers utilizing friction force microscopy and shear modulation force microscopy, and to employ the theories and background information to discuss the experimental results. The steps are:

1. Familiarize yourself with the background information provided in Section 4.
2. Test your background knowledge with the provided Quiz in Section 2.
3. Conduct the friction and force modulation experiments in Section 3. Follow the experimental step-by-step procedure.
4. Analyze your data as described in Section 3
5. Finally, provide a report with the following information:
   (i) Results section: In this section you show your data and discuss instrumental details (i.e., limitations) and the quality of your data (error analysis).
   (ii) Discussion section: In this section you discuss and analyze your data in the light of the provided background information.
       It is also appropriate to discuss section (i) and (ii) together.
   (iii) Summary and outlook: Here you summarize your findings and provide an outlook on how one could use the technique in other fields.
        The report is evaluated based on the quality of the discussion and the integration of your experimental data and the provided theory. You are encouraged to discuss results that are unexpected. It is important to include discussions on the causes for discrepancies and inconsistencies in the data.

2. Quiz – Preparation for the Experiment

Theoretical Questions

(1) (*3pts*) Determine the contact area for a JKR contact at which the contact becomes unstable.

(2) (*3pts*) Describe the two terms *solid-like* and *liquid-like* using the two simple models of Hooke's law of elasticity and Newton's law of viscosity.

(3) (*3pts*) List methods that are use to determine the glass transition temperature. What property are they actually sensitive to?

(4) (*3pts*) At the glass transition temperature, the response signal of SM-FM that is proportional to the contact stiffness is increasing noticeably. Considering that the modulus for many polymers decreases by orders of magnitude from the glassy state to the rubbery state (e.g., in the case of polystyrene PS by about 4 orders of magnitude from 10^9 N/m^2 to 10^5 N/m^2), the probing contact area of SM-FM has to increase substantially to compensate for the reduction in the material stiffness. This is based on the Herzian relationship between the contact stiffness and the modulus, i.e, $k_c = 2aE$ (for normal distortion), or $k_c = 8aG$ (for lateral distortion).
Evaluate with the Hertzian model, the relative degree of contact area increase for polystyrene.

(5) (*3pts*) Glass transition and Gibbs free energy.
   (a) Show in a V(T) diagram the distinct difference between melt/freezing transition and a glass transition
   (b) How are changes related to the specific heat and volume obtained from Gibbs free energy.

Prelab Quiz

(1) (*10 pts*) For a sinusoidal FM microscopy experiments, the input modulation amplitude A_{in} and the output signal amplitude A_{out} shall be known in volts that are applied to the piezo (PZ) and received from the photo diode (PD), respectively. The conversion sensitivity factors S_{PZ} and S_{PD} are used to convert the two signals into nanometer.
   (a) Determine formally the root mean square (RMS) amplitudes in nanometer.
   (b) With the appropriate RMS amplitudes determine the force that is acting on a cantilever with spring constant k_L.
   (c) Assuming an ideal spring model as depicted in Figure 3, what is the force acting on the sample?
   (d) Provide an expression for the sample deformation δ as function of A_{in} and A_{out}.
   (e) Express the the contact stiffness as function of δ, A_{in}, A_{out} and k_L.

(2) (a) (*5 pts*) Explain why Amontons' law is generally valid, i.e., why friction force is generally not a function of contact area. Under what types of circumstances could it be a function of contact area?

(b) (*5 pts*) Applied normal force, F_N, can be distinguished from total normal force, F_{TOT}, by the inclusion of adhesion force, F_{ADH}, in the latter term. Often, F_N and F_{TOT} must be calculated based on force distance curve data and other information. This can be accomplished according to:

$$F_{TOT} = \frac{C_N}{S}\left(F_{SP} - F_{T-B} + F_{ADH}\right) \text{ or } F_N = \frac{C_N}{S}\left(F_{SP} - F_{T-B}\right)$$

where F_{SP} is the set point signal, F_{T-B} is the out of contact normal photodiode signal, C_N is the cantilever spring constant and S is the normal sample stiffness. Calculate F_N and F_{TOT} from the following sets of data:

|	Set A	Set B
F_{SP}	10 nA	35 nN
C_N (nominal)	0.2 N/m	0.2 N/m
C_N (actual)	0.115 N/m	0.134 N/m
S	0.04 nA/nm	0.88 nm/nm
F_{T-B}	-3 nA	10 nm
F_{ADH}	12.6 nA	230 nm

Which should be used when determining friction coefficient? Why?

(3) (*10 pts*) FM microscopy utilized a function generator with a sinusoidal input modulation to the piezo. The cantilever response modulation signal $A_{out}\sin(\omega t+\phi_{out})$ is detected with a laser detection scheme by the photodiode. Because the signals are very small, i.e., within the noise level of the signal, a lock-in technique is used. The lock-in amplifier compares the photodiode signal with the input signal to the piezo, $A_{in}\sin(\omega t+\phi_{in})$, as a reference signal. Note that both signals are not only defined by their amplitude and frequency but also by their phase ϕ. The output signal of the lock-in amplifier V_{psd} is the product of two sine waves, i.e.,

$$V_{PSD} = A_{in}A_{out}\sin(\omega t+\phi_{in})\sin(\omega t+\phi_{out})$$

This signal is composed of two AC signals, one with frequency $\omega_{in}+\omega_{out}$ and $\omega_{in}-\omega_{out}$ and is heavily low pass filtered. Consequently, as in our case, only a non-zero DC signal comes through for $\omega_{in} = \omega_{out} = \omega$. In other words the lock-in technique is frequency discriminating the signal it receives based on the reference signal. The quantities that matter are the amplitudes, and the phase shift $\phi = \phi_{in}- \phi_{in}$. As the phase of the phase signal of the input signal to the piezo is arbitrary, we will define it generally as zero, i.e., $\phi_{in} = 0$. The situation described here, is illustrated in the figure below, expressing the frequency discriminated signal V_{PSD} in complex form, i.e.,

$$V_{PSD}^* = Re^{(\omega t+\phi)}$$
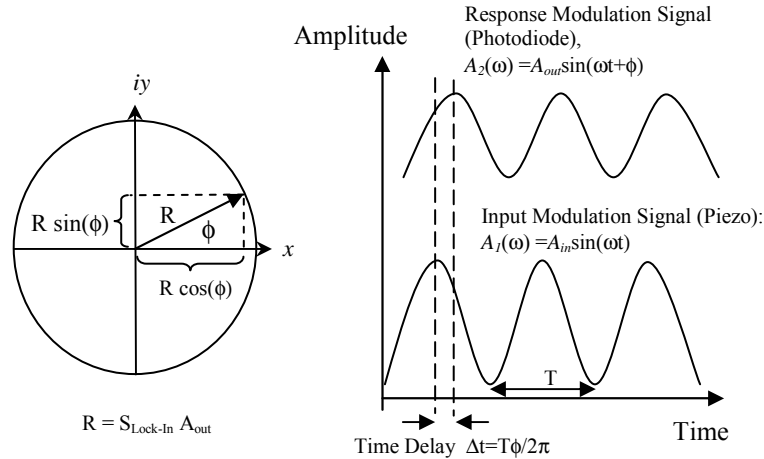
Describe the operation of the function generator. How would you expect the phase angle to differ between solid-like and liquid-like materials?

4) Below, data are provided from a friction-load experiment of Octadecyl-Phosphonic Acid (ODPA). Based on these data:

  a) Determine the shear strength properties (i.e., α and $\tau_o A$) of the materials at 29 ^{o}C and 94 ^{o}C, according to the model of Bowden/Tabor.
  b) Provide reasons for the differences in values.
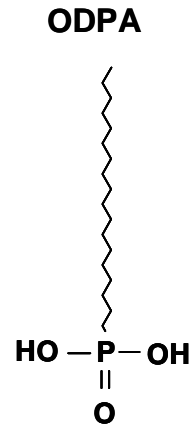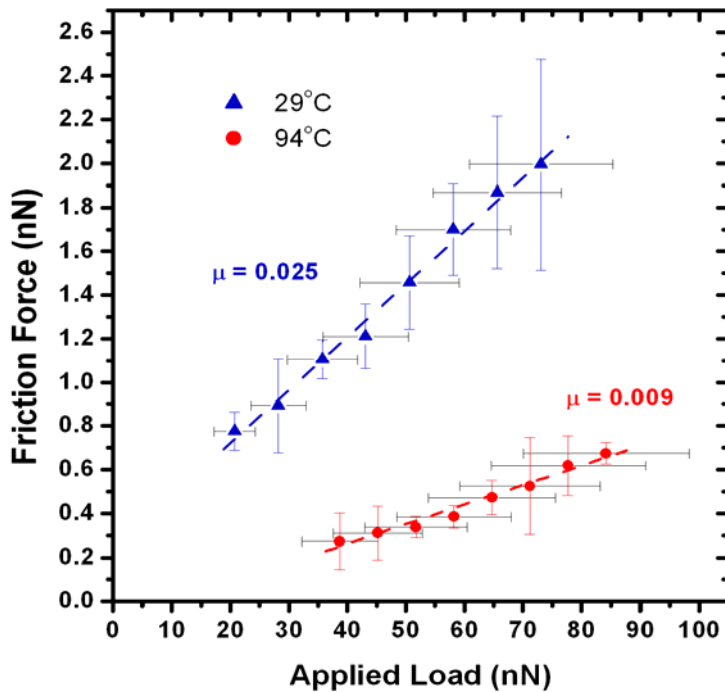
3. Experimental Assignment

Goal

Following the step-by-step instructions below, determine the glass transition temperature of the PTBA film and measure the friction coefficient as a function of temperature. Analyze and discuss the data with the background information provided in Section 4. Provide a written report of this experiment.

Specifically provide answers to the following questions:
(1) What is the observed glass transition temperature for poly (t-butyl acrylate)? Does this value correlate with the literature value? What factors would cause the observed T_g value to be different from the literature?
(2) Why is Modulated Force Microscopy effective at determining the glass transition temperature?
(3) How does the friction coefficient change as a function of temperature? Does this compare well to the results of Sills et al. for polystyrene (p. 83, lower right)?
(4) Can you determine the glass transition from the friction data? How does it compare to that obtained from the previous method?

Safety
- Wear safety glasses.
- Refer to the General rules in the AFM lab.
- The heating module should be off when it is not in use.

Instrumental Setup
- Nanosurf Easy Scan 2 Flex AFM system with long contact Mode SFM tip with 0.2 N/m spring constant with NO Aluminum coating.
- Two heating stages with controllers
- Lock-in amplifier and function generator with two long BNC cables
- Oscilloscope

Materials
- Samples: 2 pieces of pre-prepared (by TA) ~ 1cm^2 Spin-coated PtBA film on silicon substrate, stored in sealed Petri dishes until ready for the experiment. The sample PtBA ($M_w = 137.3k$) is spin cast onto an organic contaminant-cleaned (possibly also oxide treated) silicon wafer and annealed above its glass transition temperature in a vacuum oven. Preferred film thicknesses are between 100 to 500 nm.

Experimental Procedure

Read the instructions below carefully and follow them closely. They will provide you with information about (i) preparation of the experiment, (ii) the procedure for force modulation microscopy and temperature control, (iv) the procedure for friction force microscopy, (iv) the procedure for closing the experiment, and (v) how to conduct the data analysis.

(i) Preparation of the experiment
(1)   Friction force system set-up: (This part will be performed with a TA).
    a. Place PTBA sample grid on heater stage
    b. System set-up
        i.   Remove the scan head from the sample stage.
        ii. Load a Nanosensor PPP-CONT cantilever and then place the holding spring on the mount as shown below.

        iii.   Place back the mount as shown below.
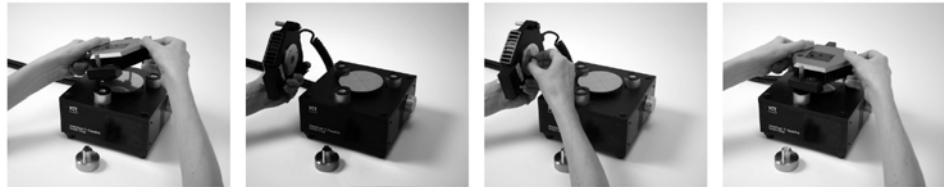
        iv. Take the SFM head and carefully place it onto the sample stage.
        v.   Crank the sample stage up until the sample is <1mm from the lever (see below). Watch this process at a 40° angle using the side view port to ensure you do not crash the tip into the sample surface.

side view port
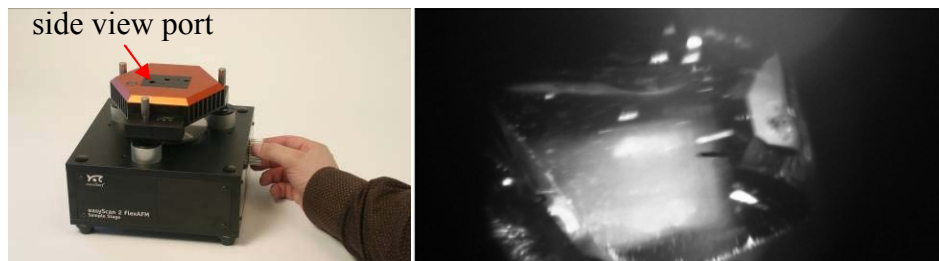
    c. Software preparation

i. Once the cantilever is loaded click on 'Operating Mode' icon in the menu list on the left side of the screen in the Easyscan 2 software. The operating mode panel will appear. Select 'CONTR' as the mounted cantilever and 'Static Force' as the operating mode.

ii. Click on the 'Imaging' icon (top right). Select the 'Topography – Scan Forward' plot. Add two new plots by clicking the new chart icon twice (middle right). Next, select one of the new charts and change the signal of the first to 'Deflection - Scan Forward' by clicking the select signal icon (bottom right) and choosing amplitude from the drop down menu. Select the second new chart and change the signal to 'Friction – Scan Forward'. Repeat this process for 'Scan Backward' plots for all three. Repeat this process again and make dual line graphs, rather than color maps for all three signals.

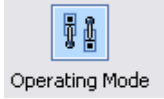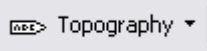(2)   Shear Modulation Force Microscopy system set-up: (This part will have been performed by the TA):

a. Place the PTBA sample on the MMR heating stage.
   i. Repeat the same procedure as above for setting up software and cantilever installation.

b. Connect BNC cables:
   i. from Function Generator *Function* output to *X-Modulation* BNC
   ii. from Function Generator Function output to Lock-In *REF IN* signal (reference)
   iii. from *X* Output BNC to Lock-In Signal *A*

(ii) Dry Dynamic Mode Imaging
1) Coming into contact:
   a. Once the cantilever is approximately 1mm from the surface, click on the 'Positioning' icon and click 'Approach' to bring the lever into contact.
   b. Close the frequency tuning window that appears.
   c. Ensure that the probe status light is green when approaching. If not, stop the approach and consult your TA for the cause of this. Note that a blinking red light means that no lever is detected, while a solid red light means that a tip is detected but the frequency is not set properly.
   d. The program will automatically switch to the imaging window once imaging begins.
2) Adjusting slope:
   a. Once imaging has begun, the slope will most likely need adjustment.
   b. This can be done automatically by selecting 'Imaging – adjust slope' from the 'Script' menu.
   c. The software automatically adjusts slope and begins the scan again.
3) Optimize scan quality:
   a. Open the Z-Controller Panel (right) by clicking the z-controller icon.
   b. Set the set point to be 50%. Use the default values for the P-Gain and I-Gain.
   c. In the Imaging Panel, change the image width to 2μm and ensure that the resolution is set to 256.
   d. Vary the set point, P-Gain, I-Gain and time/line values to optimize the image quality according to the following guidelines:
      i. Faster scan speeds (lower time/line values) generally require higher gains.
      ii. Excessively high gains cause the controller to ring, resulting in very noisy amplitude and topography signals.
      iii. Very large surface features generally require higher gains or higher amplitude or slower scan speed.
      iv. Noisy measurements may improve with increased set point, but very high set points may result in coming out of contact. You may also employ the minimum force trick, that is, increase the set point (%) until you are out of contact and then decrease it again until a reasonable image is obtained. This results in using the minimum force.
4) Obtain images:
   a. Once scan quality is acceptable complete the scan by clicking on the 'Finish' icon.
   b. If the completed image looks good, click 'Photo' and save the image.
   c. Each image should be in a different area of the sample. To move to a different area, simply select random values (from -20 to 20 μm) and input these into the 'Image X-Pos' and 'Image Y-Pos' fields in the imaging
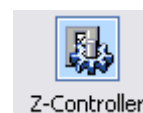
panel. Alternatively, you may withdraw the cantilever under the 'Positioning' window and use the translation stage to move to a new area of the sample surface. Be sure to 'Approach' again after moving.

    d. Click 'Start' to begin a new image. Repeat slope adjustment and image optimization as necessary.

    e. Obtain at least three images for each sample.

5) Change sample:

    a. Once all images have been obtained for that sample, go to the 'Positioning' window and click 'Withdraw'.

    b. Once the cantilever is well off the surface, click 'Retract' and raise the tip farther (~3 mm off the surface).

    c. Remove the scan head from the surface and change the sample, making sure it is appropriately grounded.

    d. Repeat steps 1)-5) for all samples.

6) Conclude imaging:

    a. Come out of contact using 'Withdraw' and 'Retract'.

    b. Remove the cantilever and store it appropriately.

    c. Shut down the Easyscan 2 software and turn off the controller.

(iii) Determining PtBA Glass Transition

(1)   Ensure that the MMR stage initial temperature is set to 300K by inputting 'SK300' into the control box. Check the temperature by typing 'TE' and pressing enter.

(2)   In the software, record the deflection signal value for out of contact. This can be performed by scanning while out of contact and watching the deflection dual line graph.

(3)   Set **PID** gains to nominal values.

(4)   Coming into contact:

    a. Once the cantilever is approximately 1mm from the surface, click on the 'Positioning' icon and click 'Approach' to bring the lever into contact.

    b. Ensure that the probe status light is green when approaching. If not, stop the approach and consult your TA for the cause of this. Note that a blinking red light means that no lever is detected, while a solid red light means that a tip is detected but the frequency is not set properly.

    c. The program will automatically switch to the imaging window once imaging begins. Click 'Stop' on the imaging panel to stop imaging.

(5)   Scan the sample surface and identify a smooth area about 5μm in size.

(6)   Ensure that the function generator settings are as follows: frequency: 4300Hz, amplitude 0.5Vpp, offset 0Vpp.

(7)   Ensure that the lock-in amplifier settings are as follows:

    i. Time Constant: 30ms, 6db.

    ii. SYNC: On.

    iii. Sensitivity: ~ 200mV, but change if the *amplitude meter bar* is too large or too small.

    iv. Signal input: A, AC, Floated Ground.

    v. Set Display: R (amplitude response), Θ (phase response).

    vi. Check initial phase shift, and set to zero (right side display)

(8)   Wait 1-2 minutes for thermal equilibrium.

(9)   By hand, record for ~30 seconds the **R** and Θ values from the lock-in.

(10)   By changing the MMR set point, repeat steps 11-15 for temperatures from 300K to 335K in increments of 2.5K

(11)   Cool the system back to 300K

(12)   Withdraw tip, set heater temperature to 300K, set function generator amplitude to 0.

(13)   Shut down the AFM system as instructed by your TA.

(iv) Determining PtBA Friction Coefficient

(1)   Ensure preparations described above have been performed.

(2)   Approach sample and come into contact per the above instructions.

(3)   Open heater software at **Desktop:contactlab:HEATER-CONTROL: TC-36-25RS232rev.A.exe**

(4)   Initialize Heater in Heater program

    a. Set **FIXED SET TEMP** to 25.00

b.   Set **SELECT COMM PORT** to COM2
c.   Click **CommCheck** (if system ready, proceed. Otherwise seek TA)
d.   Click **INITIALIZE.** Verify that **OUTPUT ON/OFF** is now **ON**

(5)   Wait 1-2 minutes for equilibrium
(6)   Ensure that the AFM is set up for forward and reverse scanning
(7)   Ensure that friction force contour maps and dual line graphs are available within the software for data analysis.
(8)   Begin scanning once equilibrium has been reached at a scan rate of 1 Hz over a scan area of 1 micron. The resolution should be 64 or lower.
(9)   For each temperature measure the friction force for 6 loads (e.g., 10, 20, 30, 40, 50, 60nN) by using the length tool on the tool bar to determine the distance between lateral signal lines within the friction force dual line graph.
(10)   Also measure force-distance curves and obtain the sensitivity (slope of the approach curve once in contact) and adhesion force. (See Force-Displacement measurements with EasyScan 2 SOP).
(11)   Record these values for each temperature:

Load (nN)	High value (mV)	Low value (mV)	S (nm/nm)	Fad (nm)
10				
20				
30				
40				
50				

(12)   Repeat (12) at least twice per temperature to obtain an idea of the error associated with the measurement.
(13)   By changing **FIXED SET TEMP** in the heater program, repeat steps 6-11 for temperatures from 25 to 50°C in increments of 2.5°C
(14)   Cool system back to 25°C
(15)   Shut down the AFM system by following the shutdown procedure described in Easy Scan 2 AFM system SOP.

(v) Instructions for Data Analysis
(1) T_g analysis
   a. Plot R vs. temperature and the identify transition onset.
   b. How large is the change in R as the sample goes through its transition?
   c. What other parameters could be investigated to maximize T_g sensitivity?
(2)   Friction data Analysis
   a. Determine the friction coefficient for each temperature by plotting the measured friction force as a function of applied load. The slope is the apparent friction coefficient.

    b. Plot the resulting friction coefficients as a function of temperature. Compare this trend to that of polystyrene for Sills et al. How are they different, how are they similar?

    c. Discuss why friction coefficient is a function of temperature. Could you predict the glass transition from the friction coefficient?

4. Background: Friction, Contact Mechanics and Viscoelastic Phenomena of Polymers

Table of Contents:

Stress-Strain Relationships

Before we begin a detailed discussion of friction and viscoelastic theory, it is important to lay out some fundamental concepts relevant to the mechanics of materials. We begin with the concept of stress. A macroscopic object can be subjected to stress when forces are applied to it. In general, there are two basic types of mechanical stress, tensile stress and shear stress, as illustrated in Fig. 1. For tensile stress, the force is exerted normal to the surface of the object, resulting in a tension stress, σ, equivalent to the normal force, F_N, divided by the initial cross sectional area of the normal surface, A_o ($\sigma = F_N / A_o$). Shear stress, τ, is applied in the same plane as the surface, and is determined by the total lateral force, F_L, divided by the initial area over which the force is applied, A_o ($\tau = F_L / A_o$).

When a stress is applied to a material, a deformation of the material generally results. Tensile deformation is conveniently described in terms of strain, ε, where strain is the change in length, δ, divided by the initial length, L_o, ($\varepsilon = \delta / L_o$). Shear strain, γ, is slightly different and is defined in two dimensions as the change in lateral distance, Δu_x, divided by the change in vertical distance, Δy, ($\gamma = \Delta u_x / \Delta y$).

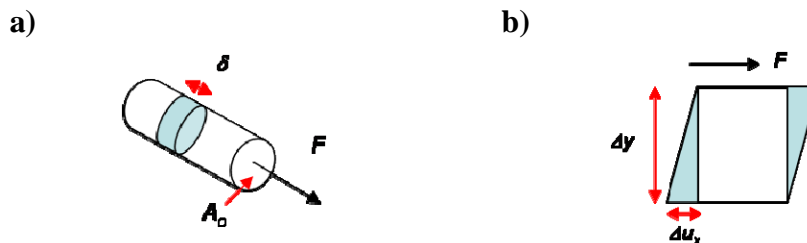a)   b)

Fig. 1. (a) tensile stress and strain and (b) shear stress and strain in two dimensions.

Figure 2 (a) provides a general diagram of stress as a function of strain in tension. As shown, deformations can behave in a number of ways over a range of stress. First, if the strain resulting from a given stress disappears when the stress is removed, then the material is said to behave elastically and stress is a linear function of strain, as shown in the early portion of the curve in Fig. 2(a). In the case of elastic behavior, energy is stored within the system and a simple equation exists relating stress to strain, called Hooke's Law after the English mathematician Robert Hooke (1635-1703):

$$\sigma = E\varepsilon \tag{1}$$

where E is the modulus of elasticity (or Young's modulus), which is a material property. Similarly, for shear stress:

$$\tau = G\gamma \tag{2}$$

where G is the shear modulus of the material. Beyond the yield point, or the elastic limit of the material, the strain will not return to zero after removal of the stress, as shown in Fig. 2(b), rather, a plastic deformation has taken place that has permanently deformed the material.
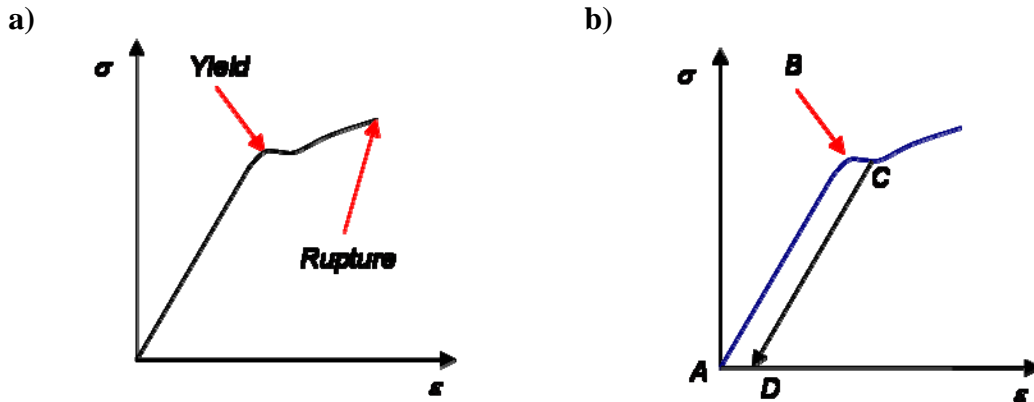
a)   b)

Fig. 2. (a) General stress-strain relationship, (b) deformation beyond yield point, B, resulting in a plastic deformation where strain does not return to zero when the stress is removed.

To round out our discussion of stress-strain relationships, we should note that when a solid material is stressed in tension, for example, strains other than the normal strain may be observed. So, when a strain is observed in the axial plane as a result of a normal stress (as in Fig. 1(a)), strain in the lateral directions are also observed as the radius of the rod "shrinks" to compensate for the elongation in length. French mathematician Simeon Denis Poisson (1781-1840) recognized this, and therefore we name the ratio of lateral strain to axial strain after him, Poisson's ratio, v:

$$v = \left| \frac{lateral\_strain}{axial\_strain} \right| \tag{3}$$

When operating in the elastic regime, it can be shown that the shear modulus and the modulus of elasticity are related to Poisson's ratio as:

$$E = 2G(1+v) \tag{4}$$

which is a useful relationship in many circumstances. Having developed a framework from mechanics of materials, we now turn our attention to understanding friction, and will eventually return to mechanics principles later on when we introduce viscoelastic theory.

Classical Understanding of Friction

The original work performed in an effort to understand friction was performed by Leonardo Da Vinci (1452-1519) and later confirmed by Guillaume Amontons (1663-1705). Amontons provided two laws with respect to macroscopic friction:

- the friction force (F_F) is proportional to the normal force (F_N),

$$F_F = \mu F_N \qquad\qquad (5)$$

 where μ is dubbed the "friction coefficient" and
- the friction force is independent of the size of the body (area of contact).

At first, these laws seem counter intuitive—why should friction not depend on the area of contact (size) of the body? Why does roughness not play a role?

Boden and Tabor explained that this phenomenon is due to the nature of contact between macroscopic surfaces. Even the smoothest macroscopic surfaces (e.g. machined metal) are rough at lengthscales approaching the atomic scale (Fig. 3(a)). Thus, when two macroscopic surfaces are brought in contact, topography differences result in very little actual, physical contact between the two surfaces (Fig. 3(b)). Since interaction forces and surface forces are very short-ranged, only the areas of contact interact with each other.

When two materials (e.g. metals) contact each other they may deform elastically or plastically if the yield pressure, P_{yield}, a property unique to each material (corresponding to the yield point in Fig. 2(a)), is exceeded. For very steep promontories, with minimal contact, elastic deformation is possible (discussed below), but often plastic deformation will occur and the material will flow at the contact point, increasing the area of contact until the true contact area is sufficient to support the applied load without further deformation (i.e. until the actual pressure, $P \leq P_{yield}$).

a)
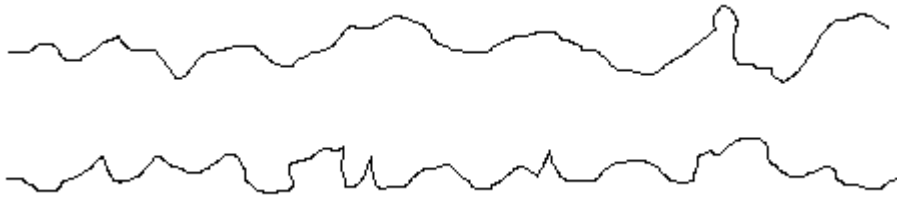
b)

Fig. 3. (a) A representation of two surfaces, rough on small lengthscales, which, when brought into contact (b) show very little actual contact area.

Therefore, in order to support an applied normal force, F_N (often the weight of the material, W), the process is as follows. The materials come into contact with an initial total contact area, A_i (the sum of all N individual initial contact areas, A_j^i), wherein the yield pressure is exceeded:

$$P = \frac{F_N}{A_i} = \frac{W}{\sum_{j=1}^{N} A_j^i} > P_{yield} \tag{6}$$

The materials then flow, increasing the total contact area to A, (the sum of all M final contact areas, A_j^f):

$$P = \frac{F_N}{A} = \frac{W}{\sum_{j=1}^{M} A_j^f} \leq P_{yield} \tag{7}$$

Coupling the first of Amontons' Laws with this equation gives:

$$F_F = \mu F_N = \mu P A \tag{8}$$

where it can be seen that if the normal force increases, the total contact area (A) also increases to maintain $P \leq P_{yield}$ as described above. Thus, to a first approximation, Amontons' Law adequately explains macroscopic friction and shows that it is not directly dependent on either size or roughness of the bodies involved.

The Bowden-Tabor Adhesion Model of Friction

More recent advances in the area of friction have been made by Frank Philip Bowden and David Tabor, who, working in the twentieth century, developed a model of friction based on adhesion by assuming that all deformations between bodies were plastic in nature. The justification for this model lies in the fact that the areas in contact with each other "adhere" to one another due to the short range interactions such as van der Waals forces. Friction must overcome these forces for motion to occur, and therefore friction is a function of the true contact area, A and a material constant called the shear strength τ_s. Within Bowden and Tabor's simple mechanical adhesive model, it is assumed that all points of contact (asperities) deform plastically during sliding. Thus, the laterally imposed shear force for sliding ("friction force") represents a critical force necessary for sliding to occur under given external conditions, such as load, sliding rate and termpature. Thereby, the imposed shear stress τ (i.e., the lateral force per unit area) is balanced by the material intrinsic shear strength, τ_s, and thus,

$$\tau = \tau_s = \frac{F_F}{A}. \tag{9}$$

The shear strength has been found to be linearly related to the applied pressure P, i.e., the load imposed on the true contact area,

$$\tau_s = \tau_o + \alpha P, \tag{10}$$

via the material specific constants τ_o and α, as provided for monolayer fatty acid systems in Table 1. By combining Eqs 9 and 10, the friction force is linearly related to the normal force (load), i.e.,

$$F_F = \tau_s A = (\tau_o + \alpha P)A \tag{11}$$

$$F_F = \left(\tau_o + \alpha \frac{F_N}{A}\right)A = A\tau_o + \alpha F_N \tag{12}$$

Amontons' law is recovered for most systems as the pressure induced shear strength component, αP, dominates the zero-pressure shear strength component in materials. However, in ultrathin films as provided in Table 1, very small α values have been found resulting in nearly pressure independent friction forces, i.e., very low (close zero) friction coefficients.

Table 1: α, τ_o values of fatty acids $(C_{n-1}H_{2n+1})COOH$

	n = 14	n = 18	n = 22
α	0.034	0.038	0.036
τ_o	0.6	0.6	2.2

Source: B.J. Briscoe et al., Proc. R. Soc. Lond. **A 380**, 389 (1982)

Models of Single Asperity Contact

The fact that the Bowden-Tabor model recovers Amontons' law is the main reason why it has been widely used to explain friction systems. The issue becomes more complex, however, for cases where there is a single point of contact between bodies, as is more nearly the case for the atomic force microscope cantilever tip in contact with a sample. Situations arise where contact is not fully plastic, but rather there is a range of possible contact, from fully elastic deformation, to deformation which is different for each body, to situations where no deformation occurs at all. The fully plastic deformation has been described above in Tabor and Bowden's theory, but in this section we will briefly mention several other approaches.

A helpful framework for all the other models has been developed by Maugis[1], and is based on the assumption that the interaction potential between a single asperity and the surface is finite in contact, with an adhesive force s_o, which is a function of separation distance, and a work of adhesion w. This results in a non-dimensional elasticity parameter, λ, as:

$$\lambda = 2s_o\left(\frac{9R}{16\pi w(E^*)^2}\right)^{\frac{1}{3}} \tag{13}$$

where R is the radius of contact, and E^* is the combined elastic modulus, further discussed below. The elasticity parameter, λ, is small for hard materials and large for soft materials. When plotted against applied load several discrete regimes are apparent as illustrated in Figure 4.
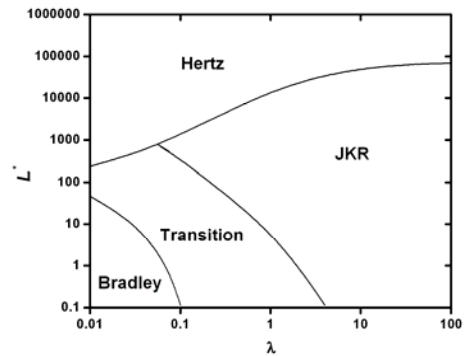
Fig 4. Illustration of the contact mechanics regimes as they vary with compressive dimensionless loading, figure extracted from literature data[2].

Two of these loading regimes, i.e., the fully elastic Hertzian regime and the adhesive-elastic JKR regime will be discussed in more detail below.

Contact Mechanics – Fully Elastic Models

Hertz analyzed the stresses at the contact of two elastic solids, and thereby assumed small strains within the elastic limit. The contact radius a is considered significantly smaller than the radius of curvature R, and the two contacting surfaces, as depicted in Fig. 5, assumed to be non-conformal. Furthermore, creep at the interface is neglected, i.e., a frictionless contact assumed.
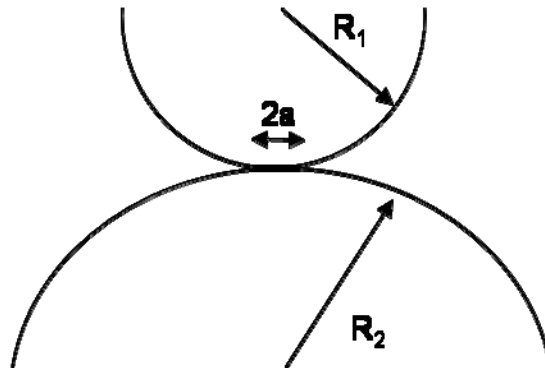

Fig. 5. Contact of two elastic spheres.

Based on this assumption, the contact radius a, the contact area A, and both the maximum pressure p_{max} and the mean pressure p_m can be determined with an elastic infinite half-space analysis as:

$$\text{Hertz contact radius: } a = \left[\frac{3LR^*}{4E^*} \right]^{1/3} \qquad (14)$$

$$\text{Hertz area of contact: } A = \pi a^2 = \pi\left[\frac{3LR^*}{4E^*}\right]^{2/3} \tag{15}$$

$$\text{Mutual approach: } \delta = \frac{a^2}{R^*}\left[1 - \frac{2}{3}\left(\frac{a_o}{a}\right)^{3/2}\right] \text{ with } a_o = a|_{L=0} \tag{16}$$

$$\text{Hertz pressure: } p_{\max} = \frac{3L}{2\pi a^2} = \frac{3}{2}p_m\left[\frac{6L\left(E^*\right)^2}{\pi^3 R^{*2}}\right]^{1/3} \tag{17}$$

with the applied normal force (load) L, and the combined Young's modulus and radius of curvature of the two materials (1 and 2), i.e.,

$$E^* = \left(\frac{1-v_1^2}{E_1} + \frac{1-v_2^2}{E_2}\right)^{-1} \text{ and } R^* = \left(\frac{1}{R_1} + \frac{1}{R_2}\right)^{-1} \tag{18 & 19}$$

where v is the Poisson ratio ($v \approx 0.5$ for polymers). For the case of a sphere-plane contact, which is most like an SFM probe and the sample surface, $R_2 \to \infty$ and therefore R^* is equivalent to R, the radius of the tip. In the Hertz model adhesive interactions are neglected, as seen at zero loads where the contact area vanishes.

The adhesion force between two rigid spheres can be expressed as:

$$F_{adh} = -2\pi R^*\Delta\gamma; \quad \Delta\gamma = \gamma_1 + \gamma_2 - \gamma_{12} \tag{20 & 21}$$

where $\Delta\gamma$ is called the "work of adhesion" per unit area. This force-adhesion relationship is named after *Bradley*. Neither elastic nor plastic deformations are considered in Bradley's model. Johnson, Kendall and Roberts introduced a very successful elastic model - the JKR model. Based on this model, the area of contact $A = \pi a^2$ can be easily deduced from the JKR contact radius, i.e.,

$$a = \left[\frac{3R}{4E^*}\left(L + 3\pi R\Delta\gamma + \sqrt{6\pi R\Delta\gamma L + \left(3\pi R\Delta\gamma\right)^2}\right)\right]^{1/3}. \tag{22}$$

Note, for vanishing work of adhesion, the JKR expression for a corresponds to the Hertzian contact radius. For non-zero adhesion forces, the significant difference of the two models is illustrated in Fig. 6. With the JKR model, a negative loading regime between L = 0 and the instability load, i.e., the adhesion force

$$L = F_{adh}^{JKR} = -\frac{3}{2}\pi R^*\Delta\gamma,$$

is possible.

Considering that the JKR adhesion force equation is seemingly independent of any elastic modulus, there seems to be an inconsistency, if compared to the Bradley model

above. The apparent discrepancy was resolved by David Tabor (1977) who introduced the following parameter:

$$\mu_T = \frac{\left(R^*\right)^{1/3}\left(\Delta\gamma\right)^{2/3}}{\sigma\left(E^*\right)^{2/3}}, \qquad \text{"Tabor Coefficient"} \qquad (23)$$

where E, and σ the characteristic atom-atom distance. The Tabor coefficient expresses the relative importance of the adhesive interaction versus the elastic deformation. For $\mu_T > 5$, which is typical for soft organic materials, the JKR model is appropriate.
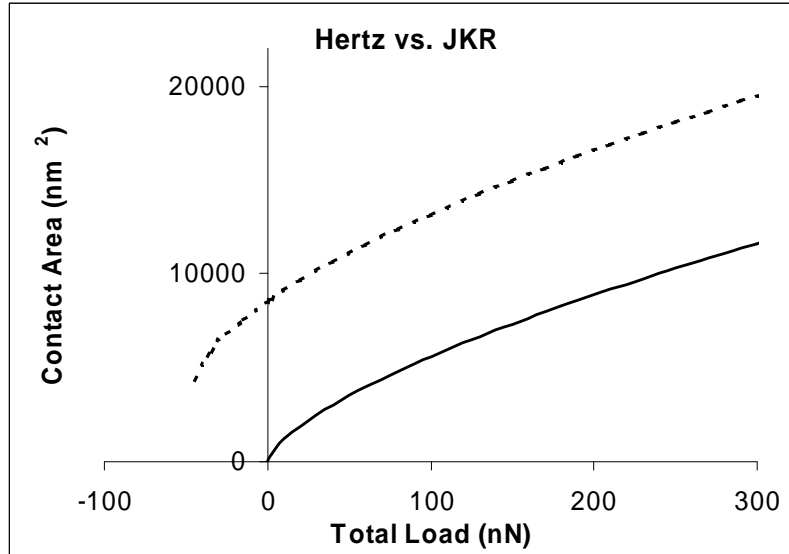

Fig. 6. Hertzian elastic contact and JKR adhesive-elastic contact as function of load.

Force Modulation SFM and Hertzian Theory

The Hertzian theory of elastic circular point contact for a planar surface and an assumed spherically caped tip, Fig. 7, describes the contact radius as

$$a = \left[\frac{3LR}{4E}\right]^{1/3}, \qquad (14)$$

where R is the radius of curvature of the probing SFM tip, and E is the modulus of the sample only, if the sample material stiffness is much smaller than the modulus of the cantilever material. The mutual relative approach of distant points δ between the sample and probing tip, i.e., the sample indentation for an incompliant tip material, is given by the Hertzian theory as

$$\delta = \left[\frac{9L^2}{16RE}\right]^{1/3} \qquad (24)$$

For a fully elastic sample and a incompliantly stiff probing SFM tip, δ reflects the elastic strain deformation (indentation) of the sample material. For a force modulated relative approach, the load varies around the equilibrium load L_o as

$$L = L_o + \frac{\partial L}{\partial \delta} \delta \qquad (25)$$

As we consider only the sample being deformed, a one-dimensional sample stiffness (generally referred to as contact stiffness) can be introduced as the derivative of the load, i.e.,

$$k_c \equiv \frac{\partial L}{\partial \delta} = \left(6E^2 L_o R\right)^{1/3} \qquad (26)$$

The equation above is synonymous with the non-adhesive Hertzian expression

$$k_c = 2aE \qquad (27)$$

Higher order derivatives provide anharmonic distortions (dissipation) that can be neglected. The equilibrium load can be expressed by the normal spring constant of the cantilever k_L and the equilibrium deflection z_o as $L_o = k_L z_o$.
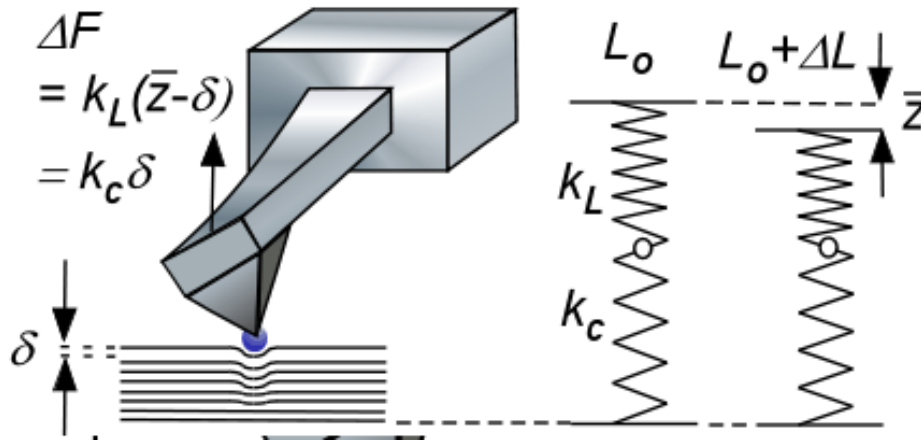

Fig. 7. Elastic sample deformation involving rigid SFM tip.

Thus, for a sinusoidal normal stress disturbance, $z = A \sin(\omega t)$, with a root mean square amplitude

$$\bar{z} = \frac{1}{\sqrt{2}} A \qquad (28)$$

the dynamic force acting on the cantilever is proportional to the net displacement (input modulation minus sample deformation), i.e.,

$$\Delta F = k_L \left(\bar{z} - \delta\right) \qquad (29)$$

In an analogous manner the force modulation can also be described from the sample perspective as

$$\Delta F = k_c \delta \qquad (30)$$

The "normal force", ΔF, acting on the SFM lever in the process of an indentation can be expressed in Hooke's limit as

$$\Delta F = k_{sys} \bar{z} = k_c \delta = k_L \Delta z_L \quad \text{with} \quad \Delta z_L = \bar{z} - \delta, \qquad (31)$$

as illustrated in Fig. 7. The system combined spring constant, k_{sys}, is then given as

$$k_{sys} = \left(\frac{1}{k_c} + \frac{1}{k_L} \right)^{-1} .$$

(32)

Analogous relationships exist also for elastic shear modulation.

Contact Stiffness

In the previous paragraph, we have assumed that only the sample is deformed and the material response is rate independent. If both bodies are compliant, the non-adhesive Hertzian contact stiffness is given as

$$k_c = 2aE^*$$

(33)

where E_i and v_i (I = 1,2) are the reduced material Young's moduli and Poisson ratios, respectively. This equation has also been found to be applicable for viscoelastic materials, i.e.,[3]

$$k_c(\omega) = 2aE^*(\omega)$$

(34)

where $k_c(\omega)$ and $E(\omega)$ reflect effective stiffnesses.

If we also consider adhesion to take place in the contact area, the Hertzian theory would have to be replaced by the JKR theory, which leads to the following expression for a normalized contact stiffness to zero load:[3]

$$\frac{k_c(\omega)}{k_c(\omega)\big|_{L=0}} = \left[\frac{1 + \sqrt{1 - L/F_{adh}}}{2} \right]^{2/3}$$

(35)

$$k_c(\omega)\big|_{L=0} = 2a_o E^*(\omega) = 2E^*(\omega) \left[\frac{9\pi R^2 \Delta\gamma}{2E^*\big|_{\omega\to 0}} \right]^{1/3}$$

(36)

Force Modulation and Polymer Relaxation Properties

Controlled temperature experiments involving force modulation microscopy provide the opportunity to investigate relaxation properties of polymeric and organic materials. Thereby, the contact stiffness is monitored as a function the temperature, as illustrated below with shear modulation force microscopy (SM-FM) employed to thin polystyrene films. Due to the small probing area even the smallest changes in the polymer internal pressure, modulus and surface energies can be detected. SM-FM is allows for accurate determination of transition properties, such as the glass transition temperature,[*] T_g, of nanoconstrained systems, such as ultrathin polymer films with a thickness below ~100 nm, Fig. 8(a).

The SM-FM method is briefly described as follows: A nanometer sharp SFM cantilever tip is brought into contact with the sample surface, Fig. 8(b). While a constant load is applied, the probing tip is laterally modulated with a "no-slip" nanometer amplitude, ΔX_{IN}. The modulation response, ΔX_{OUT}, is analyzed using a two-channel lock-in amplifier, comparing the response signal to the input signal. The modulation response,

---

[*] Background information regarding the glass transition of viscoelastic material is provided below.

i.e., the effective stiffness, is a measure of the contact stiffness. Thermally activated transitions in the material, such as the glass transition, T_g, are determined from the "kink" in the response curve, as shown in Figure 4(b).

Conceptually, the force modulation FM approach is a nanoscopic analogue to dynamic mechanical analysis (DMA). In essence, mechanical responses to external shear forces with varying temperature entail a material's viscoelastic properties, such as the modulus.
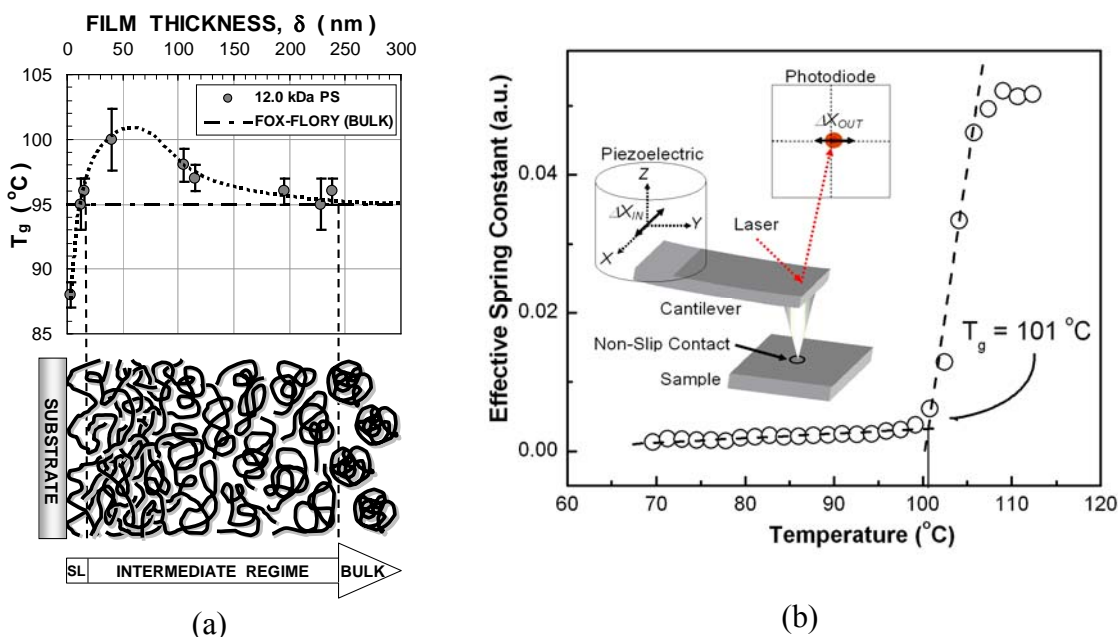

Fig. 8. (a) Nanoscale constrained glass transition profile below 100 nm thick polymer films. (b)Working principle of Shear Modulation Force Microscopy (SM-FM)

Transition and Viscoelasticity

It is hard to imagine life without plastics, looking at water bottles, car bumpers, backpacks, computer casings, and many more products that involve synthesized organic materials – called polymers. There are numerous reasons to list why the last one hundred years can be called the *Plastic Age*. Polymers are light weight, formed in any shapes and colors, and can be produced with a simple scheme at low cost. One major advantage of polymers over traditional materials such as metals is their versatility in their mechanical property. Polymers can be soft and flexible like rubber bands and chewing gums, but also stiff and tough like the aircraft body of the new Boeing 787.

One critical parameter in designing polymeric product is the glass transition temperature T_g. The glass transition can be pictured, although with some caution, as a structural order-disorder transition that is observed in non-structured (amorphous) solids. One of the main features of the glass transition is the change in the mechanical and diffusive properties of the material below and above T_g. For instance, below T_g the material starts to act stiff and is brittle (i.e., glass like), and above T_g, still in the solid (condensed) phase, it exhibits high mechanical flexibility due to the existence of molecular chain mobility. Despite the importance of the glass transition of polymeric

materials, the glass transition phenomena and its underlying viscoelastic behavior are not completely understood. These shortcomings have however not stopped mankind from designing continuously new polymer based products on a macroscopic level. However, the ambiguity in our current fundamental understanding of the glass forming process in polymers is being challenged by the recent nanotechnology spurt. As the dimension of solid systems approach the nanoscale, a dimension that is comparable to the size of polymer chains, it matters from an effective design perspective to grasp the exact relaxation mechanism behind the glass transition process.

One of today's most common ways to determine the glass transition temperature is the measurement of the change in the specific heat capacity $C_p(T)$ as a function of temperature by differential scanning calorimetry (DSC). Although widely used because of its convenience, DSC is also known for its inaccurately. One of the main reasons is that the glass transition process takes place not only at a specific temperature, like a typical first order phase transition, but over a range of temperatures[4]. Thus, T_g as determined by DSC has to be assigned, to some degree arbitrarily within a critical temperature range, as illustrated in Fig. 9. Another reason for the difficulties in determine T_g originates from the viscoelastic nature of polymers, which makes the material temperature rate dependent with a high possibility of aging during the characterization process. DSC information is usually obtained from the polymer in powder form, to reduce effects based on thermal history and process engineered properties.[5] In other words, for T_g determination, DSC is restricted to the characterization of bulk materials, like other widely used techniques, as the dynamic mechanical analysis (DMA), Fig. 9. DMA is sensitive to changes in the in-phase G' and out-of-phase modulus response G". The ratio of these two moduli components, define the loss modulus (also referred to as loss tangent tan δ), with which T_g can be identified. Due to imposed macroscopic mechanical constraints this value is may differ from a DSC calorimetric glass transition.

There is currently not only a need for new techniques to provide a more fundamental understanding of the glass transition process, but also for methods that are applicable to small scale systems; e.g., thin films, and polymeric heterosystems (e.g., polymers blends and polymer nanocomposites). A technique that has been found to address the experimental shortcomings of DSC and DMA is shear modulation force microscopy (SM-FM), as introduced above.
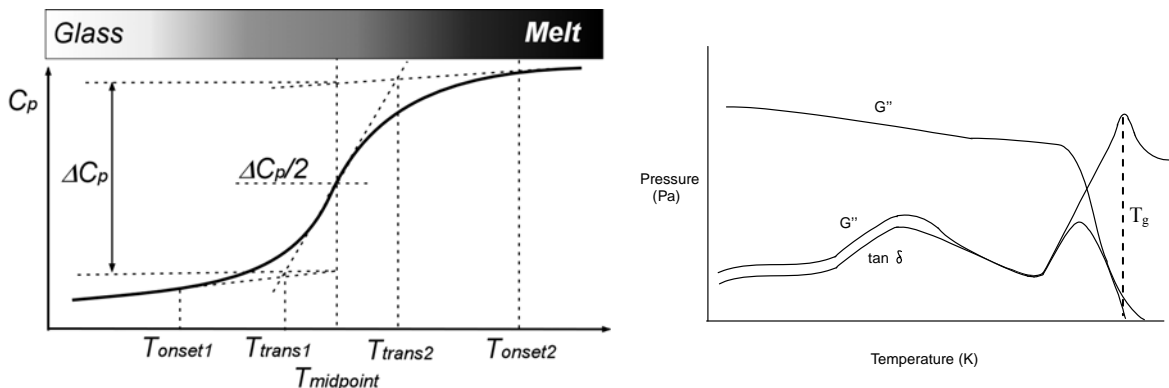

Fig. 9: (left) Schematic thermogram of $C_p(T)$. Shows the various distinct temperatures used to define the midpoint temperature T_g. (right) Schematic thermomechanical results, as obtainable by DMA.

Introduction to Linear Viscoelasticity

The science that deals with the mechanical properties of condensed phases under external stresses is called Rheology. We will limit our discussion to a subdiscipline of rheology, i.e., linear viscoelasticity, with which we conceptually separate the *liquid-like* (viscous) behavior from the *solid-like* (elastic) behavior. Thereby, a material that exhibits *ideal solid-like* behavior under stress can be described with a simple stress-strain relationship, and a material with *ideal liquid-like* behavior shows a simple stress-strain-rate dependence. With *stress* we define the external force per unit area that is imposed on the condensed phase. The resulting deformation (e.g., length or angular deformation (ΔL or γ) for a uniaxial length extension, or simple shear, respectively) defines a strain ratio (e.g., $(L_o+\Delta L)/L_o$ or $\tan \gamma$). It is convention to use for uniaxial stress and strain the Greek symbols σ and ε and for the shear stress and strain τ and γ. Strain rates reflect the time derivative of the strain.

Ideal solid-like and ideal liquid-like

Ideal solid-like materials deform and relax instantaneously with changes in the applied external stresses. *Hooke's Law*, mentioned above, is a manifestation of a solid-like behavior. Thus, an ideal solid-like behavior is synonymous with *ideal elastic*. Mechanical energy is stored in an ideal elastic material without exhibiting any form of energy dissipation. The energy is instantaneously regained with the discharge of the external stresses. The conceptual counter behavior to ideal solid-like is ideal liquid-like as found in a *Newtonian liquid*. The basic equation of simple flow is described one-dimensionally by *Newton's law of viscosity*,

$$\tau_{yx} = -\eta \frac{dv_x}{dy}, \tag{37}$$

which relates proportionally the shear force per unit area, $F_x/A = \tau_{xy}$, to the negative of the local velocity gradient (time derivative of the deformation) with a constant viscosity value, η. The velocity gradient represents a strain rate. If a stress is applied to a Newtonian liquid no strain is built up. The material is incapable of mechanical energy storage. Once the stress is removed the material does not relax. The material resistance to shear manifests itself in the rate with which the stress is imposed. In a perfect liquid we find a linear relationship between the stress and the strain rate. The proportionality factor is called *viscosity*.

In general, any realistic liquid and solid matter will behave in a mixed manner, solid-like and liquid-like, depending on the degree and time scale over which external stresses are acting.

Linear Viscoelasticity

Mixed liquid-like and solid-like characteristics of viscoelastic materials suggest that the external forces applied are partially stored and partially dissipated. This is nicely described by a simple constitutive equation based on a periodic deformation process. If the viscoelastic behavior is in a linear region, a shear sinusoidal stress that is applied to a viscoelastic body exhibits a sinusoidal strain with a phase lag that is expressed as follows:

$$\gamma = \gamma_0 \, sin(\,\omega \cdot t\,), \tag{38}$$

$$\sigma = \sigma_0 \, sin(\,\omega \cdot t + \delta\,), \tag{39}$$

ω is the angular frequency, and δ is the phase lag, and γ_0 and σ_0 are the maximum magnitudes of the strain and the stress. The expression of the sinusoidal stress can be expanded to elucidate the two components, i.e., in phase component and out of phase component,

$$\sigma = \sigma_0 \, sin(\,\omega \cdot t\,)cos(\,\delta\,) + \sigma_0 \, cos(\,\omega \cdot t\,)sin(\,\delta\,). \tag{40}$$

The in phase component, $\sigma_0 \, cos(\delta)$ is referred to as the storage modulus G', and the out of phase component, $\sigma_0 \, sin(\delta)$ is called the loss modulus G''. The stress relationship then can be expressed as

$$\sigma = \gamma_0 \cdot G' \cdot sin(\,\omega \cdot t\,) + \gamma_0 \cdot G'' \cdot cos(\,\omega \cdot t\,), \tag{41}$$

Expressed in complex notation the strain and stress are:

$$\gamma = \gamma_0 \, exp(\,i \cdot \omega \cdot t\,), \tag{42}$$

$$\sigma = \sigma_0 \, exp\big(i \cdot (\,\omega \cdot t + \delta\,)\big), \tag{43}$$

and thus, we can introduce a complex modulus G^* as,

$$\frac{\sigma}{\gamma} = G^* = \frac{\sigma_0}{\gamma_0}(cos\,\delta + i \cdot sin\,\delta) = G' + i \cdot G'', \tag{44}$$

The *storage modulus G'* represents the storage capability of the systems and the *loss modulus G''* describes the dissipation character of the system in form of plastic deformation or flow. The ratio of the loss and the storage component is referred to as the loss tangent,

$$tan\,\delta = \frac{G''}{G'}, \tag{45}$$

and reflects the relative viscous and elastic properties. The smaller the loss tangent is the more elastic is the material. $tan\delta$ is often the most sensitive indicator of various molecular motions within the material. Figure 10 provides a response visualization of a simple shear phenomenon.
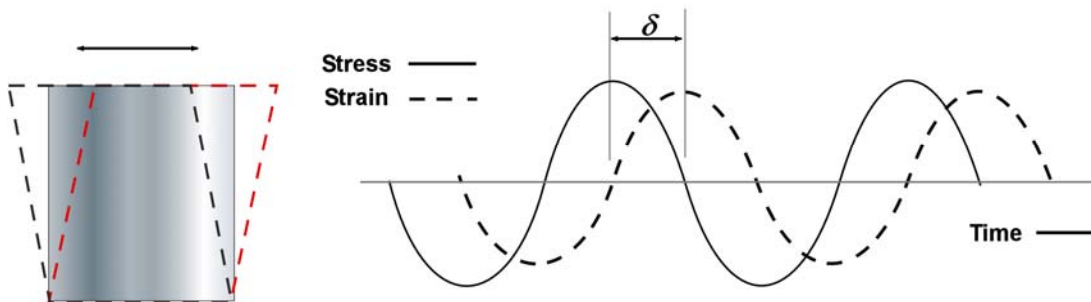

Fig. 10. Dynamic shear stress-strain visualization.

The response of a viscoelastic material can be described by a simple combination of dashpots (dissipative) and springs (elastic). The simplest model of a spring and a dashpot in series is the Maxwell's model (Fig. 11(a)) with

$$\frac{d\gamma}{dt} = \frac{1}{G}\frac{d\sigma}{dt} + \frac{1}{\eta}\sigma \tag{46}$$

where η is the viscosity, we have introduced above. The solution to this differential equation is,

$$\sigma(t) = \gamma_0 \cdot G \cdot exp\left(-\frac{t}{\eta/G*}\right) \tag{47}$$

with $G* = \sigma/\gamma$. This model predicts a time sensitive modulus, i.e.,

$$G(t) = G \cdot exp\left(-\frac{t}{\tau_\gamma}\right), \tag{48}$$

where τ_γ is the characteristic relaxation time, and t is the observation time. Thus, if the deformation process is very fast compared to the material relaxation time, i.e., t » τ_γ the elastic behavior will dominate. For very slow deformation (t « τ_γ), the system's viscous behavior dominates. Another basic viscoelastic setup is obtained by operating a spring in parallel with a viscous dashpot. (Kelvin-Voigt Model, Fig. 2(b))The Kelvin-Voigt model provides the following relationships:

$$\sigma = G \cdot \gamma + \frac{\eta \cdot d\gamma}{dt} \tag{49}$$

and the solution with a constant stress σ_0 is,

$$\gamma(t) = \frac{\sigma_0}{G}\left[1 - exp\left(-\frac{t}{\tau_\sigma}\right)\right] \tag{50}$$

where τ_σ is the retardation time of the strain.
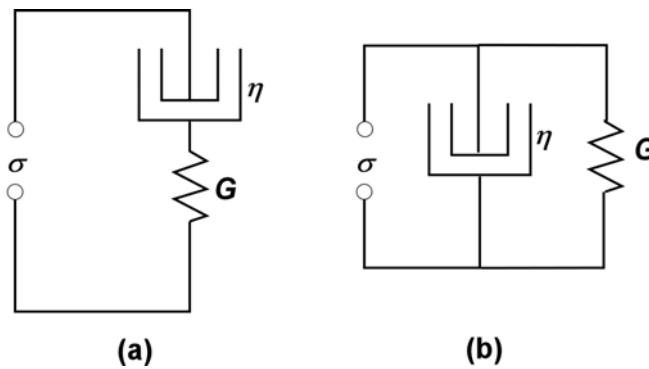

(a)   **(b)**

Fig. 11: Dashpot spring model of (a) Maxwell Model (b) Kelvin-Voigt Model.

While the Maxwell model describes the stress relaxation but not creep, the Kelvin-Voigt model describes creep but not stress relaxation. For viscoelastic material, the simplest model would be the combination of the two, [6]

$$\sigma + \left(\frac{\eta_1 + \eta_2}{G_1} + \frac{\eta_2}{G_2}\right)\frac{d\sigma}{dt} + \frac{\eta_1\eta_2}{G_1G_2}\frac{d^2\sigma}{dt^2} = \eta_2\frac{d\gamma}{dt} + \frac{\eta_1\eta_2}{G_1}\frac{d^2\gamma}{dt^2} \tag{51}$$

as G_1, G_2, η_1 and η_2 are corresponding to two springs and two dashpots, Fig. 12. If this is solved with the sinusoidal stress,

$$\frac{G'-G_0}{G_\infty - G_0} = \frac{\omega^2 \cdot \tau_\gamma^2}{1 + \omega^2 \cdot \tau_\gamma^2} \tag{52}$$

$$\frac{G''}{G_\infty - G_0} = \frac{\omega \cdot \tau_\gamma}{1 + \omega^2 \cdot \tau_\gamma^2} \tag{53}$$

$$\tan \delta_m = \frac{G_\infty - G_0}{G_0 + G_\infty \omega^2 \cdot \tau_m^2} \tag{54}$$

where G_0 and G_∞ are *relaxed* and *unrelaxed* moduli, respectively, and τ_m is derived as:

$$\tau_m = (\tau_\sigma \tau_\gamma)^{1/2} = \left(\frac{\eta_1}{G_1} \frac{\eta_1}{G_1 + G_2} \right)^{1/2} \tag{55}$$

The maximum of the loss curve then corresponds to $\tau_m \omega_0 = 1$. The product $\tau_m \omega_0$ is referred to in the literature as the Deborah number, and reflects the ratio of the externally imposed time disturbance and the intrinsic relaxation time[6]
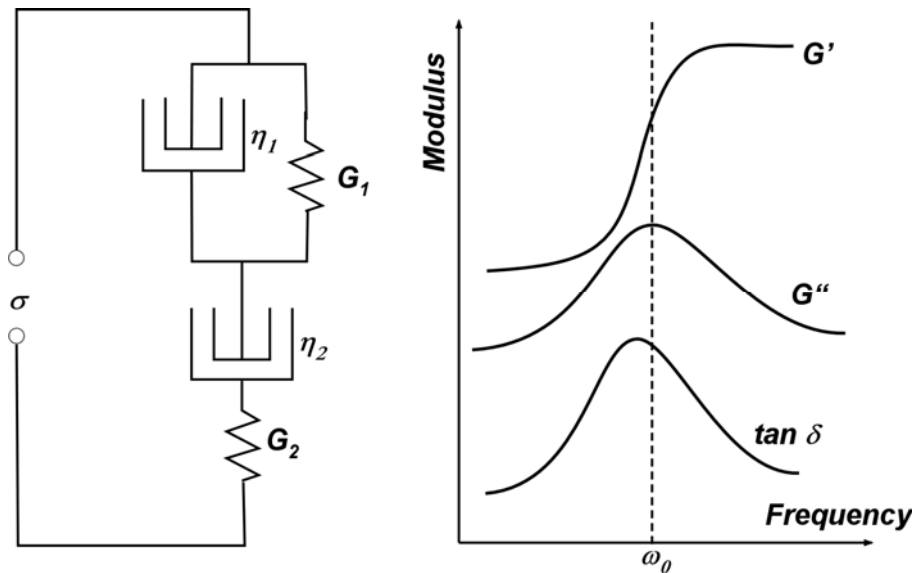

Fig. 12: A combination of the Maxwell and Kelvin-Voigt Model.

Many more combinations of springs and dashpots are possible and in detail described in the literature.[5]

Time-Temperature Equivalence of Viscoelastic Behaviors

We showed in the previous section that the viscoelastic behavior is strongly affected by the temperature and the observation time (frequency). Here the concept of time-temperature equivalence is introduced. Consider a glass window. Glass windows are made with an amorphous inorganic (silica mixture) material that appears in daily life to be "solid-like. However, it is more appropriate to consider glass to be in a highly viscous condensed phase that appears to be at equilibrium in a solid-like state during the time of observation. By controlling the temperature without imposing any transitions we can accelerate or slow down the flow process In that sense, the viscoelastic behavior of the material is affected similarly by either changes in the temperature and or time. This is called a time-temperature equivalence and is illustrated in Fig. 13. Figure 13(a) and (b) reflect the modulus in a time (i.e., frequency) domain, and in a temperature domain, respectively. Valuable information about the viscoelastic behavior of materials can be deduced from such measurements and will be discussed in the following sections.
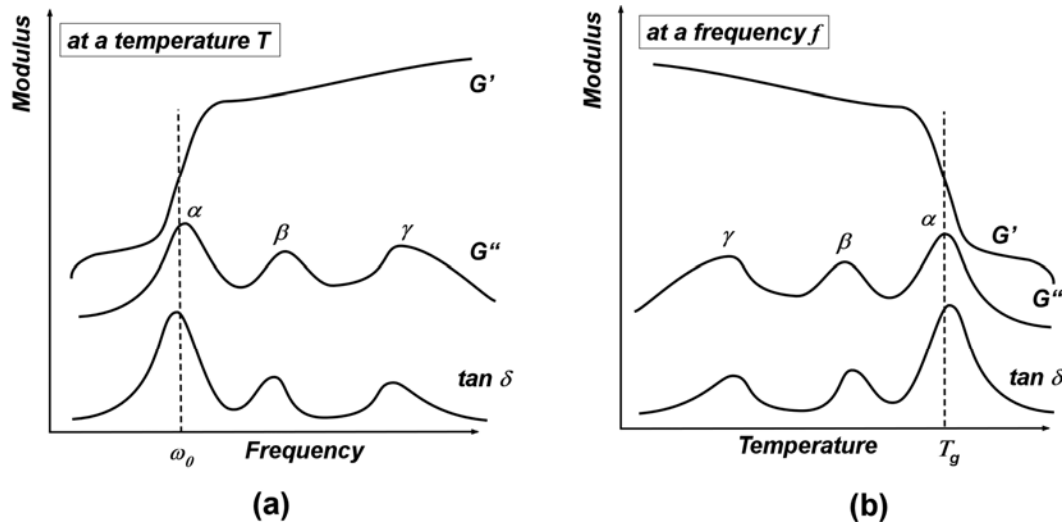
Fig. 13: Modulus spectrums in (a) time domain, and in (b) temperature domain.

Glass Transition

The *glass transition* T_g is defined as the reversible change in an amorphous material (e.g., polystyrene) or in amorphous regions of a partially crystalline material (e.g., polyethylene), from (or to) a viscous or rubbery condition to (or from) a hard and relatively brittle one. As shown in the previous section, Fig. 13(b), this transition corresponds to a temperature at which the modulus drastically changes. Above the glass transition temperature the material, still a solid, reveals a strongly rubbery behavior that is to part liquid-like. Below the transition temperature the material behaves like a brittle solid-like material. The glass transition itself, as illustrated in Figure 14, exhibits a strong cooling rate dependence and is in appearance significantly different from melting (first order phase) transition. Also the frequency of the applied macroscopic stresses is affecting the temperature of the transition.
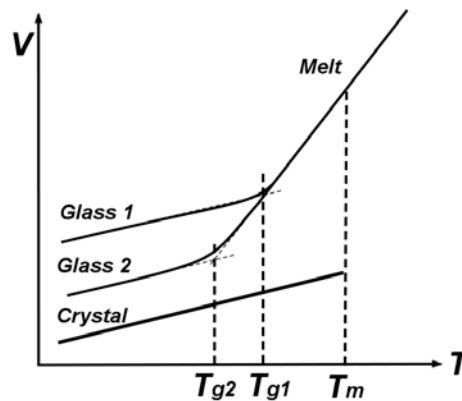

Fig. 14: Specific volume change as function of temperature. Depending on the cooling rate any liquid can freeze into a glass phase (fast quenching; e.g. of metallic glasses). Depending on the cooling rate, T_g can significantly shift as indicated with

Glass 1 and Glass 2. In polymers, the transition from a melt to a glass is not discontinuous as the first order phase transition (indicated with melting temperature T_m). Hence the assignment of a single transition value for T_g seems to be ambiguous on first sight.

Thermodynamically, the free energy changes between equilibrium states are usually identified by a discontinuity in the first partial derivatives of the Gibbs free energy G = H -TS, with respect to the relevant state variable (pressure P and temperature T), as illustrated Fig.15. Discontinuities, as expressed in the first partial derivatives of the Gibbs free energy

$$\left(\frac{\partial G}{\partial P}\right)_T = V , \tag{56}$$

$$\left(\frac{\partial G}{\partial T}\right)_P = -S , \tag{57}$$

$$\left(\frac{\partial (G/T)}{\partial (1/T)}\right)_P = H , \tag{58}$$

are found in the property-temperature relationships, i.e., the volume V, the entropy S and enthalpy H.
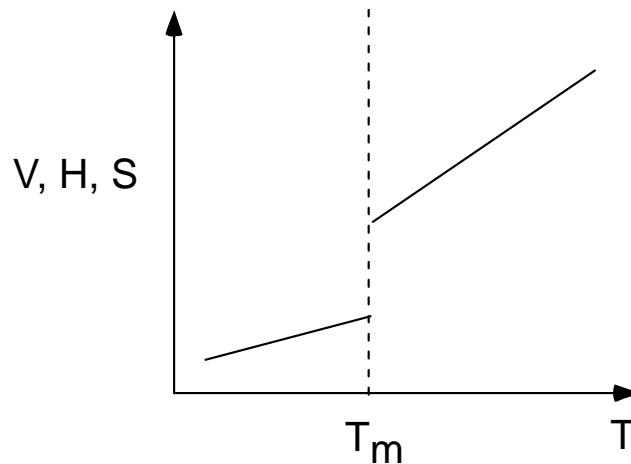

Fig. 15: Volume discontinuity. First-order transition between liquid and solid. (T_m melting temperature).

The second derivatives of the Gibbs free energy introduces the heat capacity C_p, compressibility κ and thermal expansion coefficient α.

Heat Capacity, C_p :

$$-\left(\frac{\partial^2 G}{\partial T^2}\right)_P = \left(\frac{\partial S}{\partial T}\right) = \frac{C_p}{T} \tag{59}$$

$$\frac{\partial}{\partial T}\left[\left(\frac{\partial (G/T)}{\partial (1/T)}\right)_P\right]_P = \left(\frac{\partial H}{\partial T}\right)_P = C_P \tag{60}$$

Compressibility, κ:

$$\left(\frac{\partial^2 G}{\partial P^2}\right)_T = \left(\frac{\partial V}{\partial P}\right)_T = -\kappa V \tag{61}$$

Therm. Expansion Coeff., α:

$$\left[\frac{\partial}{\partial T}\left(\frac{\partial G}{\partial P}\right)_T\right]_P = \left(\frac{\partial V}{\partial T}\right)_P = \alpha V \tag{62}$$

　　　　Figure 16 provides a rough classification based on the changes of the free energy and derivatives with temperature. While, column (i) illustrates the qualitative behavior of a first-order phase transition (i.e., a melting/freezing transition), column (ii) and (iii) are found for second order and glass transitions, respectively. A second order phase transition (e.g., an order-disorder transition) exhibits no discontinuity in V and H, and S. But there are discontinuities in C_p, κ and α.

　　　　First and second order transitions are illustrated in Figure 16. If compared to property changes in glasses around the glass transition temperature, one finds some similarity between the glass transition and the second order transition. There are however significant differences. C_p, κ and α values are always smaller and closely constant below the glass transition temperature, T_g, if compared to the values above T_g. This is in contrast to the second-order transition.
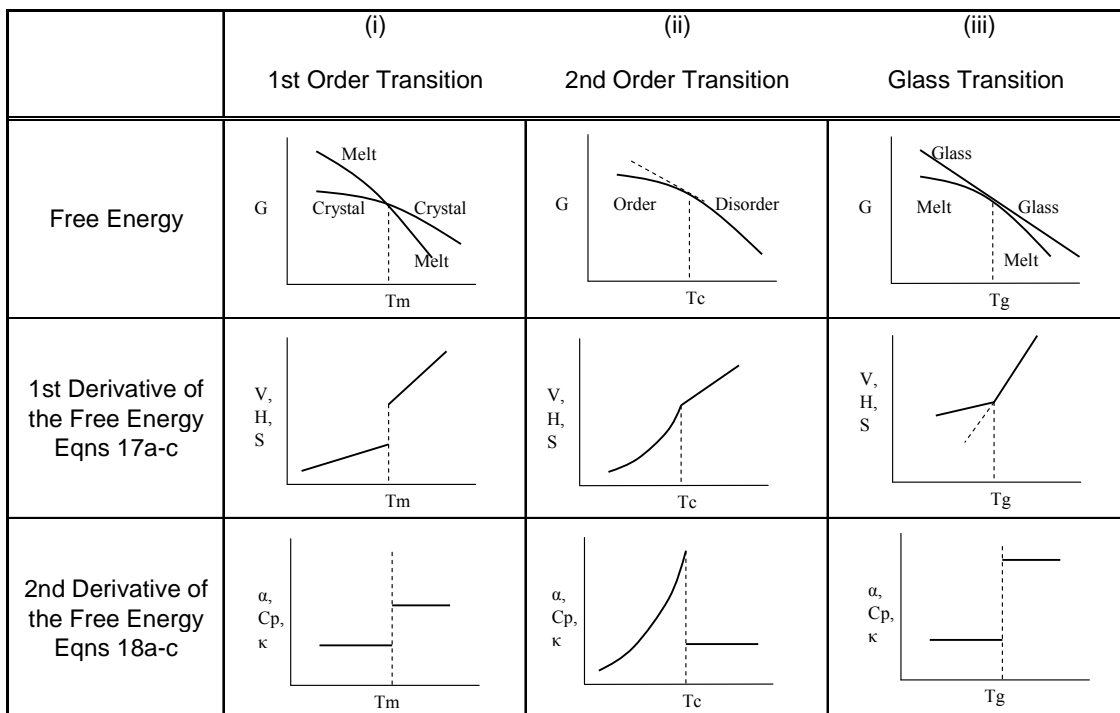

Fig. 16: Schematic representation of the changes with temperature of the free energy and its first and second derivatives for (i) first order, (ii) second order and (iii) glass transition.

References

[1]　　　D. Maugis, J. Colloid Interface Sci. **150** (1), 243 (1992).

[2]　　　K. L. Johnson, in *Micro/Nanotribology and Its Applications*, edited by B. Bhushan (Kluwer Academic Publishers, Dordrecht, 1997), pp. 151.

[3]　　　D. M. Ebenstein and K. J. Wahl, Coll. Inter. Sci. **298**, 652 (2006).

[4]　　　J. J. Aklonis and W. J. MacKnigh, *Introduction to Polymer Viscoelasticity*, 2nd Ed. ed. (Wiley-Interscience, New York, 1983).

5   D. W. Van Krevelen, *Properties of Polymers*. (Elsevier Scientific Publishing Company, Amsterdam, 1976).

6   P. Hedvig, *Dielectric Spectroscopy of Polymers*. (John Wiley & Sons, New York, 1977).

Recommended Reading

Introduction to Polymer Viscoelasticity by John J. Alkonis and William J. MacKnight, Wiley-Interscience Publication, 2nd Ed., New York, 1983.

Mechanical Properties of Solid Polymers by I. M. Ward, Wiley-Interscience Publication, London, 1971.

Nanoscience: Friction and Rheology on the Nanometer Scale by E. Meyer, R. M. Overney, K. Dransfeld, and T. Gyalog, World Scientific Publ., Singapore, 1998.